Electronic Spectra of Trigonal and Disordered Phases of Tellurium and Selenium. I. Theory

B. Kramer
Institut für Physik, Universität Dortmund, Germany

K. Maschke
Abteilung für Physik, Universität Marburg, Germany

L. D. Laude
Surface Physics Division, European Space Research Organisation, Noordwijk, Holland

(Received 20 February 1973)

The electronic density of states of trigonal and amorphous tellurium and selenium are calculated in the energy region of the two-highest-valence-band triplets and the two-lowest-conduction-band triplets. The calculations are performed using the pseudopotential scheme. The structural model for the amorphous phases is based on the assumption that the average short-range order is the same as in the trigonal crystals. The main results are that (i) the density of states of the amorphous phases of both materials is essentially structureless in the energy region of the second-conduction-band triplet; (ii) some fine structure is maintained in the two valence bands and the first conduction band. These can be associated with parts of the density of states contributed from a region of the Brillouin zone along the k_z axis. The results are compared to those obtained by using a tight-binding approximation. The comparison with experimental data will be performed in an accompanying paper.

I. INTRODUCTION

Most of the information available on the electronic structure of the trigonal form of Te and Se concerns the p bands and the forbidden band gap.[1,2] The electronic configurations of these two elemental semiconductors are $5s^2p^4$ and $4s^2p^4$, respectively. Two p bands (labeled p_1 and p_2) are located in the upper part of the valence band. The third p band (p_3) delineates the bottom of the conduction band. A gap separates p_3 from a second conduction band (SCB), which is either d like (in Te) or s like (in Se) in character. In the case of Te, p_1 and p_2 are centered 3.0 and 1.0 eV below the top of the valence band at point H, respectively. For this material, the p_2-p_3 gap is direct (at H) and of the order of 0.3 eV; the width of p_3 is approximately equal to 2 eV. In Se, all p bands are nearly twice as broad as in Te: p_1 and p_2 are centered 4.5 and 1.5 eV, respectively, below the valence-band edge at H, and the width of p_3 is some 4–4.5 eV. The main difference at this stage between the Se and Te band structures lies in the forbidden band gap. In Se, this gap (1 eV) is indirect between points H (p_2) and A (p_3), the direct gap between p_2 and p_3 at point H being equal to approximately 1.8 eV. Optical-absorption measurements[3–13] have been primarily concerned with transitions between these three p bands, and different band structures[14–21] have been tested to fit these experimental data, especially in the photon energy ranges 0–4 eV (for Te) and 0–5 eV (for Se), where p_1-p_3 and p_2-p_3 transitions can only occur. However, these measurements, while giving information on transitions between states near some critical points, do not help to locate independently these states on an absolute energy scale. The use of high-photon energies to allow excitation from core levels should in principle lead to direct information on the conduction-band states. However, as Sonntag *et al.*[22] have shown for the case of Te, the highly localized nature of the excitation leads to some uncertainty in interpretation. Photoemission has the advantage of assigning spectral features to structure in the valence- or conduction-band density of states, relative to the vacuum level of the material.[23,24]

In this study the electronic structure of both the trigonal and the amorphous phases of tellurium and selenium are investigated in the energy region of the two-highest-valence-band triplets and the second-conduction-band triplet, experimentally and theoretically. The experimental investigation was performed by using photoemission techniques. Their description is presented in detail in the following paper,[25] together with experimental results for both trigonal Se and Te and their amorphous modifications. The interpretation of the experimental results is performed in terms of the electronic density of states (DOS). Special emphasis will be placed on a comparison between the properties of the amorphous and the crystalline phases.

The theoretical investigation presented in the present paper is based on the pseudopotential band-structure theory. Pseudopotential calculations of the band structures of trigonal Se and Te were performed by R. Sandrock[15] and K. Maschke,[16] respectively. These band structures form the basis

of the present DOS calculations. In order to give a detailed assignment of the observed photoemission spectral features, it turned out to be necessary to consider the partial contributions to the total DOS from different regions of the Brillouin zone. To calculate the electronic density of states of the amorphous phases, we used a generalized pseudopotential formalism adapted to systems having no long-range order but still short-range order. The structural model used for the amorphous phases is described in Sec. II. The generalized pseudopotential method for systems with several atoms in the "short-range order cell" is sketched in Sec. III. The main result is that the density of states can be written in terms of a complex-energy-band structure quite analogous to the crystalline case. Originally, this concept was developed for disordered systems corresponding to crystals with only one atom per unit cell.[41] In the same reference,[41] application was made to an electron moving in a weak potential with small deviations from the crystalline spatial periodicity. In Refs. 42 and 43 the complex-band-structure concept was used to calculate the imaginary part of the dielectric constant of some materials. (Ref. 42: Se, Ref. 43: Ge, Si and III-IV compounds). The agreement with ϵ_2 spectra, calculated from experimental data, turned out to be quite satisfying. This encouraged us to calculate the density of states of such complicated materials as Se and Te, and to try a comparison with high-resolution photoemission data. Sec. IV contains details of the DOS computation for the crystalline and the amorphous phases. From these calculations, structure in the conduction-band DOS of the amorphous modifications of both materials is expected to weaken markedly, as well as some features of the valence-band DOS, as compared to the crystalline phases. These results are confirmed by the photoemission data of the crystalline and amorphous Te and Se films reported in Paper II. Moreover, considering the structural model underlying the calculation of the electronic energy spectra of the amorphous phases, it will be possible to draw conclusions about the atomic configuration of the amorphous films.

II. THE MODEL

The most simple approach to the calculation of the electronic properties of solids at zero temperature is to consider one electron moving in a superposition of N local atom-core potentials at sites $\vec{\rho}_1$ to $\vec{\rho}_N$:

$$V(\vec{r};\vec{\rho}_1\cdots\vec{\rho}_N)=\sum_{l=1}^{N} v(\vec{r}-\vec{\rho}_l)\ . \tag{1}$$

To solve the Schrödinger equation of the system, one needs (i) information about the form of the core potential $v(\vec{r})$ and (ii) the knowledge of the atomic positions $\vec{\rho}_1\cdots\vec{\rho}_N$.

It is impossible to determine the core potential from the properties of the microscopic constituents of a solid. To avoid a self-consistent calculation, one possibility is to use some kind of realistic ad hoc potential allowing for a solution of the Schrödinger equation. An example of this kind of core potential is the muffin-tin potential in the Korringa-Kohn-Rostoker (KKR) method for calculating energy-band structures of crystals.[26,27] A second possibility is to use an empirical and, in general, nonlocal, energy-dependent model potential, which has been chosen to fit some well-known experimental data. Using this "atomic" pseudopotential, one can predict still other properties of the system. Moreover, considering another system containing the same atoms in a different configuration, one may approach the electronic energy spectrum by using the same "atomic" pseudopotential. These empirical model potentials are well known in band-structure calculations of crystalline materials, where the atomic arrangement is known.[27,28] For the description of the electronic states within a finite energy range, for instance near the energy gap, the model potential can be approximated by a local and energy-independent potential. Its Fourier transform is slowly varying and of finite range in $\vec{k}$ space. It is this kind of local, energy-independent atomic model potential, that we shall use in the determination of the electronic properties of disordered solids. As an example, Fig. 1 shows the pseudopotential of tellurium as obtained from a comparison of optical data with band-structure results.[16]

Fortunately, considering the structural properties of solids, the situation is not quite so difficult as in the case of the atomic potential. Principally, the atomic structure of a solid system can be investigated by using x-ray or neutron-diffraction methods. In the case of a crystal, where the atoms

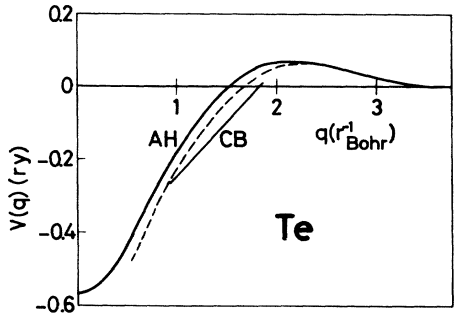

FIG. 1. Fourier-transformed atomic potential of Te (form factor). AH: pseudopotential calculated by Animalu and Heine (Ref. 5). CB: pseudopotential used by Cohen and Bergstresser (Ref. 5). Dashed line: form factor used in the calculations of this paper.

are situated at the sites of a periodic lattice, the atomic arrangement is characterized by the position vectors of atoms in the unit cell $\vec{a}_1 \cdots \vec{a}_m$ and the basis vectors $\vec{b}_1 \cdots \vec{b}_3$ of the Bravais lattice. These can be determined by analyzing Laue diagrams. The case of a disordered system is more complicated because x-ray scattering gives only information about the radial two-atom distribution.[29] This is due to the lack of long-range order. The radial two-atom distribution $P(r)$ gives the number of atoms in a spherical shell of radius r and thickness one, i.e., this function yields the numbers and distances of first-, second-, third-, etc., nearest neighbors to any fixed atom. It is obvious that one can have the same coordination numbers using different microscopic structural models. The distinction between these different microscopic models may be achieved only with additional information about the lengths and angles of the bonds connecting one atom to its neighbors. It is reasonable to assume, that in an amorphous phase the mean values of bond angles and lengths are approximately the same as in the crystalline phase. This implies, that, on the average, the amorphous system exhibits the same short-range order as the crystalline system. Disorder, i.e., the lack of long-range order, is introduced by small statistical variations of bond lengths and angles about their mean values. Additional difficulties may arise when a material exists in various crystalline modifications characterized by nearly the same arrangement of first-nearest neighbors, but a different configuration of second-, third-, etc., nearest neighbors. Therefore, a characterization of the disordered phases of such materials would require a detailed analysis of small-angle diffraction data and additional information from other experiments, such as NMR and Raman studies. In addition, the occurrence of different disordered modifications, depending on preparation conditions, cannot be excluded.[30–34]

The problem is to formulate quantitatively the above qualitative statements concerning the structural properties of disordered solids. For a crystal at zero temperature, the radial two-atom distribution function can be calculated from the probability density function:

$$p_2^0(\vec{r}) = \frac{1}{m} \sum_{(\vec{R}_n, \vec{a}_l, \vec{a}_k)} \delta(\vec{r} - \vec{R}_n - \vec{a}_l + \vec{a}_k) \tag{2}$$

by averaging it over all directions of $\vec{r}$ and multiplying by $4\pi r^2$. $\vec{R}_n$ are the lattice vectors. For a disordered structure with the same short-range order as in the crystal, we assume

$$p_2^\alpha(\vec{r}) = \delta(\vec{r}) + \frac{1}{m} \sum_{(\vec{R}_n + \vec{a}_l - \vec{a}_k) \neq 0} f_\alpha(\vec{r}; \vec{R}_n + \vec{a}_l - \vec{a}_k) , \tag{3}$$

where $f_\alpha(\vec{r}; \vec{R}_n + \vec{a}_l - \vec{a}_k)$ are localized at $\vec{R}_n + \vec{a}_l - \vec{a}_k$ with a width $\lambda(\vec{R}_n + \vec{a}_l - \vec{a}_k)$. The localization of $f_\alpha(\vec{r})$ is necessary to ensure the presence of short-range order. To relax long-range order, $\lambda(\vec{R}_n + \vec{a}_l - \vec{a}_k)$ has to increase with increasing $|\vec{R}_n + \vec{a}_l - \vec{a}_k|$. For practical reasons we choose $f_\alpha(\vec{r})$ to be Gaussian-like, i.e.,

$$p_2^\alpha(\vec{r}) = \delta(\vec{r}) + m^{-1} \sum_{(\vec{R}_n + \vec{a}_l - \vec{a}_k) \neq 0} \times \left(\frac{1}{\pi \alpha r}\right)^{3/2} \exp\left(-\frac{(\vec{r} - \vec{R}_n - \vec{a}_l + \vec{a}_k)^2}{\alpha^2 r^2}\right) . \tag{4}$$

For $\alpha \ll 1$, the half-widths of $p_2^\alpha(\vec{r})$ is about $\alpha |\vec{R}_n + \vec{a}_l - \vec{a}_k|$. For $\alpha \to 0$, we have $p_2^\alpha(\vec{r}) \to p_2^0(\vec{r})$. We may define the radius of a sphere of short-range order by

$$R_0 = a_0 / 2\alpha , \tag{5}$$

with a_0 the distance between next-nearest neighbors in the crystal. When increasing the disorder parameter α, the region of short-range order decreases. Omitting the δ function and averaging Eq. (4) over all directions of $\vec{r}$, we obtain the radial two-atom distribution:

$$P(r) = 4\pi r^2 p_2^\alpha(r) = m^{-1} \pi^{-1/2} \times \sum_{(\vec{R}_n + \vec{a}_l - \vec{a}_k) \neq 0} \frac{1}{\alpha |\vec{R}_n + \vec{a}_l - \vec{a}_k|} \times \left[\exp\left(-\frac{(\vec{r} - |\vec{R}_n + \vec{a}_l - \vec{a}_k|)^2}{\alpha^2 r^2}\right) - \exp\left(-\frac{(\vec{r} + |\vec{R}_n + \vec{a}_l - \vec{a}_k|)^2}{\alpha^2 r^2}\right)\right] . \tag{6}$$

The only natural form of tellurium is trigonal. In that atomic configuration (Fig. 2), Te atoms are arranged along parallel helical chains located at the center and corners of a two-dimensional hexagonal network. These chains are weakly bound to each other via van der Waals–like forces, while the character of the interatomic bonding within a chain is covalent. The space group of trigonal Te is $D_3^4(P3_121)$ or $D_3^6(P3_221)$, depending on the direction of the screw axis along the chains. The lattice parameters are given in Table I, together with the interatomic distances between first-, second-, third-, and fourth-nearest neighbors. Among the eight third-nearest neighbors, six of them belong to adjacent chains, the corresponding interatomic distance being equal to the lattice parameter a, which is defined as the distance between the axes of two adjacent chains. In tellurium, this distance happens to nearly equal the distance between two second-nearest neighbors belonging to the same chain.

Two crystalline forms of selenium are known: trigonal and (α or β) monoclinic. The latter will not be considered in this work, in spite of the fact that it may be important for the explanation of the

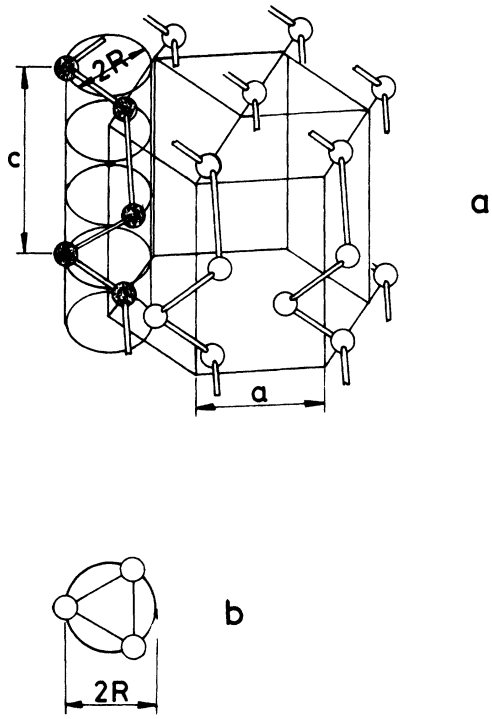

FIG. 2. Structure of trigonal tellurium and selenium. (a) Configuration of chains being situated at the center and the corners of a hexagon. (b) Top view of a chain.

short-range order in disordered Se.[30–34] The lattice parameters and interatomic distances of trigonal Se are given in Table I. The main difference between the trigonal lattices of Se and Te concerns the third-nearest neighbors. The interatomic distance between the two second-nearest neighbors in the same chain in Se is *smaller* than the distance between two adjacent chains, so that there exist only *two* third-nearest neighbors. This peculiarity reflects the fact that the interchain distance is *relatively* larger in Se than in Te and is responsible for the more molecular character of the chain configuration of trigonal Se, compared to trigonal Te.[36–38]

For the structure of amorphous Te[35] and Se, we use the trigonal configuration as a starting point. We calculated the radial atomic distribution for different values of α, i.e., different stages of disorder. The results are shown in Fig. 3(a) for tellurium and in Fig. 3(b) for selenium. For Se, we plotted also the atomic distribution obtained from x-ray diffraction.[29–31] It is clear, that it is not possible to reproduce correctly the experimental curve obtained for amorphous Se using the trigonal approach without changing the lattice parameters. The experimental distance between second-nearest neighbors in disordered Se is slightly larger than in trigonal Se. One would get a reasonable fit to the experimental curve for $\alpha = 0.07$ by increasing the interchain distance a. This would allow a better fit to the position of the third-nearest neighbors.

In the case of Te a very recent experimental atom-distribution curve, obtained by small-angle electron diffraction on films deposited and studied at low temperature, is available.[39] Comparing the experimental curves in Ref. 39 with the calculated curves in Fig. 3(a), one remarks, that the disagreement between the experimental and calculated curves for second-, third-, etc., neighbors is larger than in the case of Se, indicative of a very large degree of disorder in such films. In that case, to get a better fit, one should probably not start from the trigonal Te crystal to describe the structure of these disordered films. However, for less disordered films, one may use the model atom distribution presented above, which describes essentially a randomly disturbed crystal, and calculate the density of states in such a configuration. Then, tracing the various density-of-states features with the disorder parameter α, one may try (i) to find out those features which are mainly determined by the configuration of the nearest neighbors, and (ii) to associate them with some well identified spectral features occurring in disordered Te films.

There is one interesting point which can be observed by tracing the atom distribution curves with α. For high values of α ($\alpha > 0.13$), the two peaks in the calculated atom distributions belonging to the two first- and the four second-nearest neighbors merge into one broad peak containing six atoms. The atomic distribution is then quite similar to the one we would obtain starting from a simple cubic Te crystal with six first- and twelve second-nearest neighbors. This point will be discussed in the following paper.[25]

III. COMPLEX BAND-STRUCTURE EQUATIONS

In this section we will briefly sketch the generalized pseudopotential method used for the calculation of the density of states of the amorphous phases. Details can be found in Refs. 40–43. The density of states is given by

TABLE I. Lattice parameters (Refs. 36 and 37) and first-, second-, third-, and fourth-nearest-neighbors (Ref. 38) distances in trigonal Te (Ref. 36) and Se (Ref. 37). The number of neighbors is given in parenthesis: (+) denotes neighbors belonging to the same chain and (*) denotes neighbors belonging to adjacent chains.

	trigonal Te	trigonal Se
a (Å)	4.4572	4.3662
c (Å)	5.929	4.9536
2R (Å)	2.346	1.968
bond angle (°)	103.2 ± 0.1	103.1 ± 0.2
r(1st near. neighb.) (Å)	2.835 (2 +)	2.373 (2+)
r(2nd near. neighb.) (Å)	3.495 (4*)	3.436 (4*)
r(3rd near. neighb.) (Å)	4.457 (2+ + 6*)	3.717 (2+)
r(4th near. neighb.) (Å)	4.8921 (4*)	4.3662 (6*)

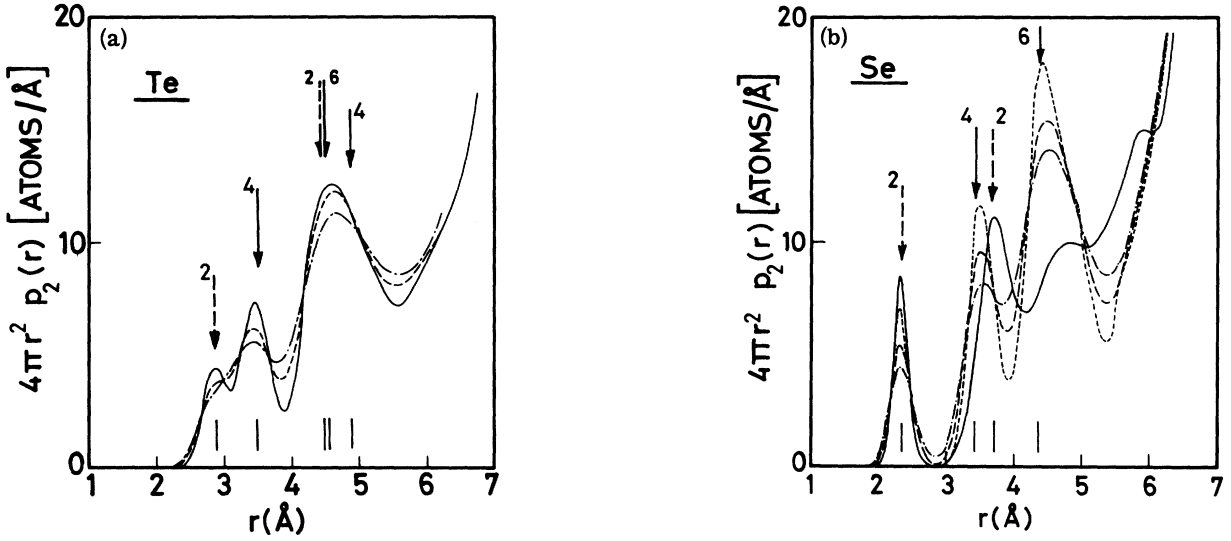

FIG. 3. (a) Radial atomic distribution function of Te for various disorder parameters α. Full line: $\alpha = 0.09$; dashed line: $\alpha = 0.11$; dashed-dotted line: $\alpha = 0.13$. The figures and arrows denote the numbers and positions of the first-, second-, third-, etc., nearest neighbors of an atom at $r = 0$. Dashed arrows denote neighbors within the same chain. Heavy arrows denote neighbors in adjacent chains. (b) Radial atomic distribution function of Se for various disorder parameters α. Dotted line: $\alpha = 0.07$; dashed line: $\alpha = 0.09$; dashed-dotted line: $\alpha = 0.11$; full line: experiment, Ref. 29. The meaning of the arrows is the same as for Se.

$$n(E) = -\pi^{-1}\mathrm{Tr}\{\mathrm{Im}G(E^+)\}, \tag{7}$$

where $G(E^+)$ is the propagator of the electron moving in the potential $V(\vec{r}; \vec{\rho}_1 \cdots \vec{\rho}_N)$ of the atom cores. $G(E^+)$ can be expressed an an infinite series:

$$G(E^+) = G_0(E^+) + G_0(E^+)VG_0(E^+) + G_0(E^+)VG_0(E^+)VG_0(E^+) + \cdots . \tag{8}$$

$G_0(E^+) = (E^+ - H_0)^{-1}$ is the propagator of the free electron. V depends on the position of the atoms. In general, it is impossible to know the exact atom positions. Therefore, we have to average the DOS over all possible configurations, hence, to average $G(E^+)$. In principle, the probability of finding a configuration $\vec{\rho}_1 \cdots \vec{\rho}_N$ is given by our structural model. Performing the averaging process and summation of the series Eq. (8) requires, however, the calculation of multiple scattering terms, i.e., terms where an electron is scattered several times at a cluster of several atoms.[44-47] These "molecule" terms make it impossible to sum the series without further approximations.

The main assumption involved in the summation of the series is that the n-atom correlation function belonging to a term of nth order in Eq. (8) can be written as a product of two-atom correlation functions[41,48]:

$$D_n(\vec{\rho}_1 \cdots \vec{\rho}_n) = \sum_{l_1 \cdots l_n = 1}^{m} D_2(\vec{\rho}_1 - \vec{\rho}_2 + \vec{a}_{l_1} - \vec{a}_{l_2}) \times \cdots \times D_2(\rho_2 - \rho_3 + a_{l_2} - a_{l_3}) \times D_2(\vec{\rho}_{n-1} - \vec{\rho}_n + \vec{a}_{l_{n-1}} - \vec{a}_{l_n}) , \tag{9}$$

where $\vec{a}_1 \cdots \vec{a}_m$ are the sites of atoms in the cluster, the multiple scattering contribution of which is treated correctly by this approach. The Fourier transformed n-atom correlation function is of the form:

$$C_n(\vec{k} - \vec{k}_1, \vec{k}_1 - \vec{k}_2, \cdots, \vec{k}_{n-1} - \vec{k}') = \sum_{l_1 \cdots l_n = 1}^{m} h_{l_1 l_2}(\vec{k} - \vec{k}_1) \times h_{l_2 l_3}(\vec{k} - \vec{k}_2) \cdots h_{l_{n-1} l_n}(\vec{k} - \vec{k}_{n-1})\, \delta(\vec{k} - \vec{k}') , \tag{10}$$

where the terms $h_{l_1 l_2}(\vec{p})$ are the Fourier-transformed two-atom correlation functions. Assuming the two-atom correlation function D_2 of Eq. (9) to be localized near the crystalline lattice points, we have their Fourier transform $h_{ll'}(\vec{p})$ localized near the reciprocal lattice points $\vec{K}_\nu$. It is convenient to choose $h_{ll'}(\vec{p})$ to be a sum of Gaussians:

$$h_{ll'}(\vec{p}) = \frac{1}{\Omega} \exp[i\vec{p}(\vec{a}_l - \vec{a}_{l'})] \left[\sum_{\nu=0}^{N_0} \left(\frac{1}{\pi\alpha K_\nu} \right)^{3/2} \times \exp\left(- \frac{(\vec{p} - \vec{K}_\nu)^2}{\alpha^2 K_\nu^2} \right) + \sum_{\nu=N_0+1}^{\infty} \left(\frac{1}{\pi\alpha K_{N_0}} \right)^{3/2} \times \exp\left(- \frac{(\vec{p} - \vec{K}_\nu)^2}{\alpha^2 2_{K N_0}^2} \right) \right]. \tag{11}$$

(Here Ω is the volume of the unit cell). With $\alpha \ll 1$ and $|\vec{K}_{N_0}| \ll (1/\alpha)(2\pi/a)$ (a is the diameter of the unit cell) we can take $e^{i\vec{p}(\vec{a}_l - \vec{a}_{l'})} \approx e^{i\vec{K}_\nu(\vec{a}_l - \vec{a}_{l'})}$. Then

we obtain from Eq. (10) for $n=2$ the Fourier transformed two-atom distribution:

$$C_2(\vec{p}) = \frac{1}{m\Omega}\sum_{ll'}\left[\sum_{\nu=0}^{N_0}\exp[i\vec{K}_\nu(\vec{a}_l-\vec{a}_{l'})]\left(\frac{1}{\pi\alpha K_\nu}\right)^{3/2}\right.$$
$$\times\exp\left(-\frac{(\vec{p}-\vec{K}_\nu)^2}{\alpha^2K_\nu^2}\right)+\sum_{\nu=N_0+1}^{\infty}\exp[i\vec{K}_\nu(\vec{a}_l-\vec{a}_{l'})]$$
$$\left.\times\left(\frac{1}{\pi\alpha K_{N_0}}\right)^{3/2}\exp\left(-\frac{(\vec{p}-\vec{K}_\nu)^2}{\alpha^2K_{N_0}^2}\right)\right]. \qquad (12)$$

Fourier transformation for Eq. (4) would yield nearly the same expression. The replacement of $\exp[i\vec{p}(\vec{a}_l-\vec{a}_{l'})]$ by $\exp[i\vec{K}_\nu(\vec{a}_l-\vec{a}_{l'})]$ is equivalent to taking into account the multiple-scattering properties of the atom cluster $\vec{a}_1\cdots\vec{a}_m$ only approximately. This is obvious from the fact that the only δ function appearing in Eq. (4) is at $\vec{r}=0$. Transformation of the correct expression Eq. (11) into $\vec{r}$ space yields additional δ function at $\vec{r}=\vec{a}_l-\vec{a}_{l'}$, i.e., the multiple-scattering contribution of the cluster $\vec{a}_1\cdots\vec{a}_m$ is treated exactly.

By writing the electron propagator of Eq. (8) in $\vec{k}$ representation and averaging it over all configurations using the correlation functions of Eq. (10), one can sum the series geometrically, assuming the atomic potential to be slowly varying in $\vec{k}$ space.[41] The result is a configurational-averaged (c.a.) electron propagator given by

$$\langle G(\vec{k},E;\vec{\rho}_1\cdots\vec{\rho}_N)\rangle_{\text{c.a.}} = g(\vec{k},E) = \frac{\det|\,\phi^{-1}(\vec{k},E)-w\,|^{(0)}}{\det|\,\phi^{-1}(\vec{k},E)-w\,|}\,, \qquad (13)$$

where $M=[\phi^{-1}(\vec{k},E)-w]$ denotes the matrix

$$M_{nn'}=[\phi_n^{-1}(\vec{k},E)\,\delta_{nn'}-w_{nn'}]\,, \qquad (14)$$

and $[\phi^{-1}(\vec{k},E)-w]^{(0)}$ is the matrix $M_{nn'}$, with $nn'\neq 0$. The function $\phi_n(\vec{k},E)$ is given by[41,46]

$$\phi_n(\vec{k},E)=\left(\frac{1}{\pi\alpha K_n}\right)^{3/2}\int d^3q\exp\left(-\frac{(\vec{k}+\vec{K}_n-\vec{q})^2}{\alpha^2K_n^2}\right)$$
$$\times\frac{1}{E^+-q^2}=\frac{i}{2}\,\frac{\sqrt{\pi}}{\alpha\,|\,\vec{k}+\vec{K}_n\,|}\,\frac{1}{|\,\vec{k}+\vec{K}_n\,|}$$
$$\times\{e^{-z_1^2}[1+\psi(iz_1)]-e^{-z_2^2}[1+\Psi(iz_2)]\}\,, \qquad (15)$$

with

$$z_{1,2}=(\sqrt{E}\pm|\,\vec{k}+\vec{K}_n\,|)/\alpha\,|\,\vec{K}_n\,|\,,$$

and $\Psi(z)=\int_0^z dy\,e^{-y^2}$ is the well-known error function. $w_{nn'}=\langle\vec{K}_n\,|\,W\,|\,\vec{K}_{n'}\rangle$ are the plane-wave matrix elements of the potential of the atom cluster $\vec{a}_1\cdots\vec{a}_m$, known from band calculation for the crystalline case.

$$w_{nn'}=\sum_{j=1}^{m}\exp[-i(\vec{K}_n-\vec{K}_{n'})\vec{a}_j]\,v_{nn'} \qquad (16)$$

(v being the atomic potential). The density of states and the dielectric constant can be written as a sum over the poles of $g(\vec{k},E)$ obtained by solving

$$\det|\,\phi_n(\vec{k},E)\,\delta_{nn'}-w_{nn'}\,|=0\,. \qquad (17)$$

Actual calculations require this determinant to have a finite dimension, so that Löwdin corrections[49] to the potential have to be taken into account:

$$\tilde{w}_{nn'}(\vec{k},E)=w_{nn'}+\sum_{\nu_1}w_{n\nu_1}\phi_{\nu_1}w_{\nu_1n'}$$
$$+\sum_{\nu_1\nu_2}w_{n\nu_1}\phi_{\nu_1}w_{\nu_1\nu_2}\phi_{\nu_2}w_{\nu_2n'}\,, \qquad (18)$$

$\nu_1,\nu_2\cdots=N\cdots\infty$, N being the dimension of the determinant. The effective potential of Eq. (18) can be obtained by subdividing the infinite $\vec{K}_\nu$ sums appearing in the series of $g(\vec{k},E)$ into two parts: $\sum_{n=0}^{\infty}\cdots\to\sum_{\nu=0}^{N}\cdots+\sum_{\nu=N+1}^{\infty}$ and partial summation of the series. For $N=1$ we have, from Eq. (17),

$$E-k^2-\tilde{w}_{00}(\vec{k},E)=0\,, \qquad (19)$$

where $\tilde{w}_{00}$ is essentially the self-energy of the system. For $\alpha=0$ we have

$$\phi_n(\vec{k},E)=[E-(\vec{k},\vec{K}_n)^2]^{-1}=G_0(\vec{k},E)\,, \qquad (20)$$

and Eq. (17) is reduced to the well-known pseudopotential equation for the energy band structure of a crystal yielding real energies $E_m(\vec{k})$ for real $\vec{k}$ vectors. In that case, the self energy $\tilde{w}_{00}$ is real. For $\alpha\neq 0$ the $\phi_n(\vec{k},E)$ have finite imaginary parts near $E=(\vec{k}+\vec{K}_n)^2$. Therefore the roots $\epsilon_m(\vec{k})$ of Eq. (12) are located in the complex energy plane if $\vec{k}$ has been chosen to be real. The self-energy is here complex. For $\alpha\ll 1$ one can assume $\epsilon_m(\vec{k})\approx\epsilon_m(\vec{k}+\vec{K}_n)$ for $\vec{K}_n$ with nonvanishing residues of $g(\vec{k},E)$. Then, the DOS can be written

$$n(E)=-\frac{1}{\pi}\sum_m\int_{BZ}d^3k\,\mathrm{Im}\left(\frac{1}{E-\epsilon_m(\vec{k})}\right)\,. \qquad (21)$$

If the real parts of $\epsilon_m(\vec{k})$ equal $E_m(\vec{k})$, the crystalline band structure, and if the imaginary part of $\epsilon_m(\vec{k})$ is approximately independent of $\vec{k}$, Eq. (21) represents the lifetime-broadened "crystalline" DOS.

IV. COMPUTATION OF ELECTRONIC ENERGY SPECTRA

A. Computational Details

1. Crystalline Case

Details of the selenium DOS calculations were presented elsewhere[50,51] and are essentially identical to the ones used in this work for Te. This section is therefore mainly restricted to the Te problem. In order to get reasonable pseudopotential form factors, the procedure adopted here is similar to Sandrock's[15] approach when performing his calculations on trigonal selenium. The actual tellurium form factors are interpolated and extrapolated from those given by Cohen and Bergstresser[52] for their ZnTe band-structure calculations. A good

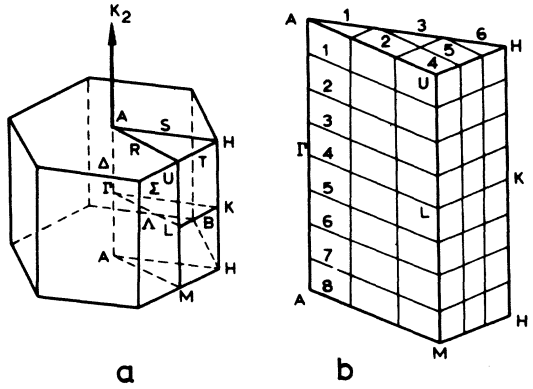

FIG. 4. (a) Brillouin zone of trigonal Te and Se; (b) irreducible wedge of the Brillouin zone.

fit to the experimental gap of 0.3 eV at point H has been obtained by slightly shifting the resulting form factors towards those obtained by Animalu and Heine[53] (Fig. 1) for Te [see also Ref. 16].

In Fig. 4 the Brillouin zone of trigonal Te is shown together with its irreducible wedge *AMH-AMH*. Because of symmetry properties, the band-structure calculation can be restricted to this part of the Brillouin zone. The irreducible wedge has been divided into 48 subzones, as shown in Fig. 4(b). For the crystalline case[16] eigenvalues were calculated in the center of the corresponding cubes using the following secular equation:

$$\det\left|\left[(\vec{k}+\vec{K}_n)^2-E\right]\delta_{nn'}+v(\vec{K}_n-\vec{K}_{n'})+\sum_\gamma \frac{v(\vec{K}_n-\vec{K}_\gamma)\,v(\vec{K}_\gamma-\vec{K}_{n'})}{E-(\vec{k}+\vec{K}_\gamma)^2}\right|=0\ , \qquad (22)$$

which is easily derived from Eq. (17), together with the first two terms of the right-hand side of Eq. (18) for $\alpha=0$. As seen in Eq. (22), plane waves corresponding to $\vec{K}_n$ and $\vec{K}_{n'}$ have been taken into account exactly, while plane waves corresponding to $\vec{K}_\gamma$ have been taken into account by first-order Löwdin perturbation theory.[49] The K_n's and $K_{n'}$'s are restricted to a sphere by the conditions

$$(\vec{k}+\vec{K}_n)\le E_1 \quad\text{and}\quad (\vec{k}+\vec{K}_{n'})^2\le E_1\ ,$$

whereas the $\vec{K}_\gamma$'s are restricted to a shell by the condition

$$E_1<(\vec{k}+\vec{K}_\gamma)^2<E_2\ .$$

To obtain a reasonable convergence, the values adopted for E_1 and E_2 were set to be 3.5 and 5.4 Ry, respectively. Using these values, 70 to 80 plane waves were taken into account exactly, and a further 70 to 80 plane waves were included by first-order Löwdin perturbation theory. To avoid computational difficulties, the energy E occurring in the denominator of the perturbation term in Eq. (22) has been replaced by a constant $E=0.45$ Ry, which lies within the gap. This is at least sufficient for the valence and the conduction bands around the fundamental gap. The higher conduction bands turned out to be very insensitive to the choice of E.

For calculation of the crystalline density of states a Monto Carlo method was used. Hitherto, in Eq. (21) the integration in $\vec{k}$ space has been replaced by a summation over N_k random $\vec{k}$ vectors:

$$n(E)=n(m\,\Delta E)\simeq\frac{1}{N_k}\sum_{i=1}^{N_k}\sum_n \delta^{\Delta E}(E_n(\vec{k}_i)-E)\ , \qquad (23)$$

with

$$m\Delta E<E\le(m+1)\,\Delta E \quad\text{and}\quad \Delta E=\tfrac{1}{300}\ \text{Ry}\ ,$$

and

$$\delta^{\Delta E}(E_n(\vec{k}_i)-E)=1 \quad\text{for}\quad |E_n(\vec{k})-E|\le\tfrac{1}{2}(\Delta E)\ ,$$
$$=0 \quad\text{elsewhere}\ .$$

$n(E)$ is then obtained as a histogram function, the mesh of the histograms being defined by ΔE. N_k is the number of random $\vec{k}$ points within the irreducible wedge. With $N_k=20\,000$, the convergence has turned out to be rather good. The eigenvalues for this large number of $\vec{k}$ points were interpolated from the results obtained for the 48 points within the irreducible wedge [Fig. 4(b)]. The upper two p-valence bands and the two-lower-conduction-band triplets were taken explicitly into account.

2. *Amorphous Case*

The complex poles of the averaged Green's function for the amorphous case were calculated according to Eq. (17). Because of the very-high-dimensional secular determinants it was necessary to replace the correct first-order Löwdin perturbation term, as given in Eq. (18), by the crystalline one [see Eq. (22)]. With this approximation, only the main diagonal elements of Eq. (22) have to be recalculated. The zeros of the determinant are calculated for the two p-valence bands and the lower two conduction bands in Γ, A, H, and K. The calculations were done for several values of α in order to investigate the band structure variations when increasing disorder. The amorphous density of states [see Eq. (21)] can be written

$$n^{am}(E)=\sum_m\sum_{k_i}\pi^{-1}\int_\infty dE'\,n^{cryst}(E',\vec{k}_i,m)\times\mathrm{Im}\{[E'-E-i\Gamma_m^\alpha(k_i)]\}^{-1}\ . \qquad (24)$$

$n^{cryst}(E,\vec{k}_i,m)$ is the contribution to the crystalline DOS arising from the band m and from a region of the Brillouin zone $\Omega(\vec{k}_i)$, where the imaginary parts of energy $\Gamma_m^\alpha(\vec{k})$ are only slightly k dependent and can be approximated by a constant. For the

actual calculations the Brillouin zone (BZ) was divided into three regions. The region about the Δ axis was defined to be the cylinder of radius $\pi/3a$ around the Δ axis. It contains about $\frac{1}{14}$ of the BZ volume. Further, the neighborhood of point H having approximately the same volume was defined by cutting out spheres of radius $\pi/2c$ around the H points. The rest of the BZ was taken as the third region.

The imaginary parts $\Gamma_m^{\alpha}(\vec{k}_i)$ for these three regions were calculated as follows: The arithmetic average of the imaginary parts at points Γ and A was taken for the Δ-axis region. For the H neighborhood we used the values at H, and for the rest of the BZ we took the arithmetic average of the values at all the four points Γ, A, H, and K.

In the Te case we had to take into account a relative shift of the real parts of the energy with respect to the valence band edge for the p_1 valence band triplet near Δ, which, for $\alpha = 0.13$, is about 0.3 eV to higher energies. This was done by shifting the Δ-axis contribution to the DOS from these bands by the same amount.

In the case of amorphous Se the DOS calculation was performed quite similarly. There are two differences, however. First, when calculating the complex Se band structure we used an approximation for $\phi_m(\vec{k}, E)$ from which no reliable information about the shifts of real parts of energy[42] can be obtained. Therefore, no shift of the real parts of energy was taken into account in this case. Secondly, the bottom of the second conduction band is not contributed by the regions near Δ and H but by the region of the BZ around $\Gamma - K$ (Fig. 6). Therefore, we subdivided the DOS into two parts: one (from 6.3 to 6.9 eV) that is contributed by the middle part of the BZ containing the axis $\Gamma - K$,[51] and the other (above 6.9 eV) contributed by all the BZ. For the $\Gamma - K$ DOS contribution below 6.9 eV, the average imaginary parts of energy are relatively small compared to those of the rest of the band (see Fig. 6 and Tables II and III).

TABLE II. (a) Complex poles $\epsilon_m(\vec{k})$ of the configurational-averaged Green's function of Te for various values of the disorder parameter α. $\epsilon_m(\vec{k})$ are calculated as the roots of Eq. (17). For $\alpha = 0$ (crystalline case) the poles E_0 are situated at the real-energy axis. For $\alpha \neq 0$ E and Γ denote the real part and imaginary part of energy, respectively. E_0, E, Γ are given in Ry. $\vec{k} = (0,0,0)$, $\vec{k} = (0,0,1)$, $\vec{k} = (1,0,1)$, and $\vec{k} = (\frac{1}{2},1,0)$ correspond with Brillouin-zone points Γ, A, H, and K, respectively. (b) Complex poles $\epsilon_m(\vec{k})$ of the configurational-averaged Green's function of Se from Ref. 40.

(a)

α			0	0.07		0.09		0.13	
			E_0	E	Γ	E	Γ	E	Γ
$\vec{k}$ - [000]		Γ_1	$0.31_{(2)}$					0.28 0.28	0.000 0.000
		Γ_2	0.315					0.29	0.005
		Γ_3	$0.38_{(2)}$	0.37 0.37	0.003 0.003	0.365 0.365	0.003 0.004	0.348 0.348	0.007 0.007
		Γ_4	0.426	0.41	0.000	0.405	0.000	0.385	0.003
		Γ_6	$0.52_{(2)}$	0.50 0.50	0.000 0.000	0.50 0.50	0.002 0.002	0.473 0.473	0.003 0.007
		Γ_8	0.585	0.55	0.000	0.540	0.001	0.51	0.005
		Γ_7	0.98	0.95	0.05	0.95	0.075		
		Γ_8	$1.03_{(2)}$	1.03 1.03	0.02 0.02	1.04 1.04	0.04 0.04		
$\vec{k}$ - [001]		A_1	0.255					0.228	0.001
		A_2	$0.315_{(2)}$					0.285 0.285	0.001 0.001
		A_3	0.395	0.382	0.000	0.376	0.000	0.355	0.003
		A_4	$0.402_{(2)}$	0.390 0.390	0.000 0.000	0.385 0.385	0.000 0.000	0.360 0.360	0.001 0.001
		A_5	0.498	0.484	0.000	0.474	0.001	0.447	0.008
		A_8	$0.508_{(2)}$	0.495 0.495	0.000 0.000	0.485 0.485	0.001 0.001	0.465 0.465	0.008 0.008
		A_7	0.99	1.025	0.012	1.046	0.025		
		A_8	$1.07_{(2)}$	1.08 1.095	0.013 0.01	1.10 1.14	0.025 0.030		
$\vec{k}$ - [101]		H_1	0.205					0.172	0.01
		H_2	$0.215_{(2)}$					0.176 0.176	0.015 0.015
		H_3	0.419	0.407	0.002	0.398	0.003	0.375	0.01
		H_4	$0.450_{(2)}$	0.437 0.437	0.000 0.000	0.429 0.431	0.002 0.002	0.405 0.405	0.009 0.009
		H_5	0.475	0.468	0.002	0.462	0.006	0.440	0.015
		H_6	$0.552_{(2)}$	0.535 0.535	0.001 0.001	0.524 0.526	0.003 0.003	0.495 0.495	0.01 0.01
		H_7	1.06	1.065	0.07	1.065	0.09		
		H_8	$1.11_{(2)}$	1.135 1.14	0.05 0.06	1.145 1.155	0.07 0.08		
$\vec{k}$ - [$\frac{1}{2}$10]		K_1	$0.23_{(2)}$					0.205 0.205	0.02 0.007
		K_2	0.295	0.293	0.001	0.285	0.002	0.275	0.06
		K_3	$0.305_{(2)}$	0.293 0.300	0.001 0.005	0.295 0.297	0.012 0.007	0.277 0.285	0.027 0.013
		K_4	0.335	0.322	0.000	0.313	0.003	0.295	0.01
		K_5	$0.600_{(2)}$	0.58 0.58	0.000 0.000	0.570 0.570	0.000 0.000	0.540 0.540	0.005 0.005
		K_6	0.610	0.593	0.001	0.582	0.001	0.547	0.005
		K_7	1.015	1.025	0.05	1.025	0.06		
		K_8	$1.06_{(2)}$	1.07 1.07	0.05 0.05	1.07 1.07	0.10 0.10		

(b)

α			0	0.075		0.10	
			E_0	E	M	E	M
$\vec{k}$ - [000]		Γ_1	0.20	0.20	0.00	0.20	0.00
		Γ_2	$0.25_{(2)}$	0.25 0.25	0.00 0.00	0.25 0.25	0.00 0.00
		Γ_3	$0.39_{(2)}$	0.39 0.39	0.00 0.00	0.39 0.39	0.005 0.005
		Γ_4	0.515	0.515	0.00	0.515	0.005
		Γ_5	$0.74_{(2)}$	0.74 0.74	0.01 0.01	0.745 0.745	0.04 0.04
		Γ_6	0.76	0.76	0.015	0.76	0.06
		Γ_7	$1.07_{(2)}$	1.07 1.07	0.02 0.02	1.07 1.08	0.035 0.03
		Γ_8	1.16	1.16	0.035	1.15	0.025
$\vec{k}$ - [001]		A_1	0.11	0.11	0.00	0.11	0.00
		A_2	$0.25_{(2)}$	0.25 0.25	0.00 0.00	0.25 0.25	0.00 0.00
		A_3	$0.41_{(2)}$	0.41 0.41	0.00 0.00	0.41 0.41	0.005 0.015
		A_4	0.48	0.48	0.005	0.48	0.02
		A_5	0.61	0.61	0.015	0.605	0.035
		A_6	$0.73_{(2)}$	0.73 0.73	0.03 0.03	0.73 0.73	0.07 0.075
		A_7	1.10	1.14	0.05		
		A_8	$1.14_{(2)}$	1.19	0.075		
$\vec{k}$ - [101]		H_1	0.01	0.01	0.00	0.01	0.00
		H_2	$0.19_{(2)}$	0.19 0.19	0.003 0.003	0.19 0.19	0.005 0.005
		H_3	0.465	0.455	0.01	0.47	0.03
		H_4	$0.545_{(2)}$	0.54 0.54	0.005 0.01	0.54 0.54	0.015 0.03
		H_5	0.695	0.695	0.015	0.69	0.055
		H_6	$0.80_{(2)}$	0.80 0.80	0.04 0.05	0.80 0.81	0.075 0.105
		H_7	1.10	1.10	0.01	1.105	0.025
		H_8	1.19	1.19	0.02	1.205	0.03
		H_9	1.28	1.29	0.04	1.29	0.08
$\vec{k}$ - [$\frac{1}{2}$10]		K_1	$0.10_{(2)}$	0.10 0.10	0.00 0.00	0.10 0.10	0.00 0.00
		K_2	0.345	0.355	0.003	0.365	0.005
		K_3	$0.37_{(2)}$	0.37 0.37	0.01 0.01	0.37 0.375	0.03 0.035
		K_4	0.44	0.44	0.03	0.44	0.065
		K_5	$0.855_{(2)}$	0.855 0.855	0.02 0.02	0.86 0.86	0.08 0.08
		K_6	0.895	0.895	0.025	0.89	0.08
		K_7	1.045	1.04	0.03	1.05	0.08
		K_8	$1.185_{(2)}$	1.18 1.18	0.06 0.06	1.18 1.18	0.16 0.20

TABLE III. Averaged imaginary parts of energy, $\Gamma_m^{\alpha}(\vec{k}_1)$ (in Ry), used in the calculation of the averaged DOS of (a) Te and (b) Se. p_1 and p_2 are the two valence-band triplets (see Figs. 7 and 8), p_3 is the lowest conduction-band triplet and SCB the second conduction-band triplet. H, Δ denote the k-space regions near the Brillouin-zone point H and near the axis $\Gamma - A \simeq \Delta$. BZ- $(H+\Delta)$ is the rest of the Brillouin zone. (For details see text.) In the case of Se (b) the lower edge of SCB spreads from 6.2 to 6.9 eV (compare also the Se band structure in Fig. 6, region $K-\Gamma$).

(a) Te

		P_1	P_2	P_3	SCB
	H	0.0075	0.005	0.008	0.08
α = 0.11	Δ	0.0005	0.001	0.003	0.08
	BZ -(H+Δ)	0.006	0.006	0.0045	0.08
	H	0.015	0.009	0.012	0.125
α = 0.13	Δ	0.002	0.004	0.006	0.125
	BZ -(H+Δ)	0.009	0.01	0.008	0.125

(b) Se

		P_1	P_2	P_3	SCB
	H	0.000	0.01	0.03	
α = 0.075	Δ	0.000	0.000	0.015	
	BZ (H+Δ)	0.005	0.015	0.025	
	lower edge				0.015
	rest of the band				0.045
	H	0.005	0.03		
α = 0.10	Δ	0.000	0.01		
	BZ -(H+Δ)	0.01	0.04		
	lower edge			0.045	0.04
	rest of the band			0.07	0.08

B. Results

The resulting band structure for crystalline Te is shown in Fig. 5. An ϵ_2 calculation based on this band structure,[16] is in good agreement with the experimental curves. Therefore, one may conclude that the over-all band structure is correct, the upper conduction band alone being shifted 1–1.5 eV to higher energies when compared with the photoemission data reported in Paper II. This inaccuracy of the band structure is due to the fact that the upper conduction band is not as well described

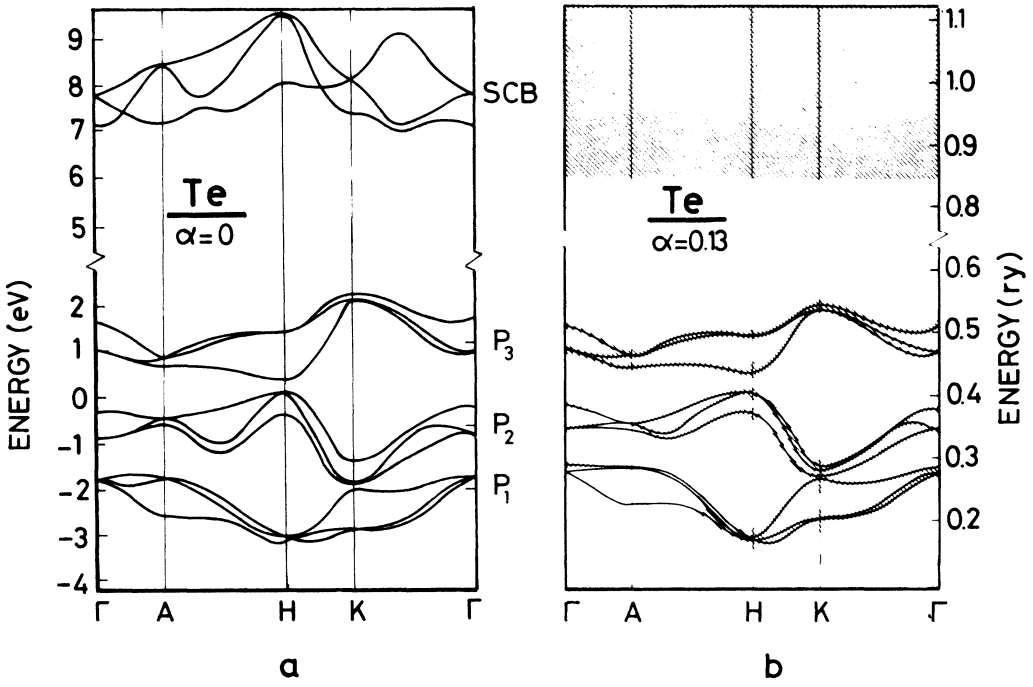

FIG. 5. Band structure of Te. (a) $\alpha = 0$: crystalline case, Ref. 16; (b) $\alpha = 0.13$: as calculated from Eq. (17). Full lines denote the real part of energy. The width of the shaded region is twice the imaginary part of energy. The second conduction-band triplet is indicated as a shaded region because the imaginary parts of energy are comparable with the width of this band.

by the same local pseudopotential as the p bands around the fundamental gap.

The band structure for amorphous Te obtained with $\alpha = 0.13$ is also shown in Fig. 5. Because of the large imaginary parts for the upper three conduction bands, there is no sense in drawing a band structure in that case. Therefore only the position of these bands is shown by the shaded area. The complex energies for different α's are listed in Table II(a). As mentioned above, near the Δ axis the real parts of the energy of the lower valence-band triplet are shifted about 0.3 eV to higher energies with respect to the crystalline band structure, whereas there is no considerable shift along the other axis. The gap between the real parts of energy at H turns out to be about 0.2 eV larger than in the crystalline case. This trend is in agreement with experimental result.[54] As mentioned earlier, the imaginary parts of the energy are very large for the second conduction band. For the upper two valence bands and the lower conduction band the imaginary parts are very small along the Δ axis, compared to other regions of the BZ.

For completeness, we show also the band structures of crystalline and amorphous Se in Fig. 6. The crystalline band structure ($\alpha = 0$) has been calculated with the same convergency stage as in the ϵ_2 calculation of Ref. 15, but differs slightly from the band structure published by Sandrock in that paper for which he used a better convergency stage. The complex band structure obtained for $\alpha = 0.075$ has been calculated in Ref. 42 by using an approximative expression for $\phi_n(\vec{k}, E)$. Some numerical results for $\epsilon_m^\alpha(\vec{k}) = E_m^\alpha(\vec{k}) + i\Gamma_m^\alpha(\vec{k})$ in Se are given in Table II(b). Figure 7 shows the crystalline and amorphous tellurium DOS together with the partial contributions from the Δ-axis neighborhood and from the region near H. The average imaginary parts of energy $\Gamma_m^\alpha(\vec{k}_t)$ used in the calculations for $\alpha \neq 0$ are listed in Table III. Comparison of the crystalline and amorphous DOS shows that the main features of the valence-band DOS and of the first conduction band are well preserved up to $\alpha = 0.11$. The remaining fine structure in the energy region of these three p bands is due to the Δ contribution, which is only slightly broadened by increasing the disorder parameter α. It is interesting to note that the shift to higher energy of the Δ contribution to the p_1 band that occurs when increasing α, gives rise to an increase of the total DOS between 1.4 and 2.0 eV [Fig. 7(a)], i.e., in the lower section of p_2. Simultaneously, the high-energy region of p_2 is depleted because of increasing imaginary parts of energy near H. The DOS of the second conduction band is completely smoothed out owing to large imaginary parts of energy for reasonable values of the disorder parameter.

Figure 8 shows the DOS of crystalline and amorphous Se calculated by using the average imaginary parts of energy listed in Table III. The DOS of Se

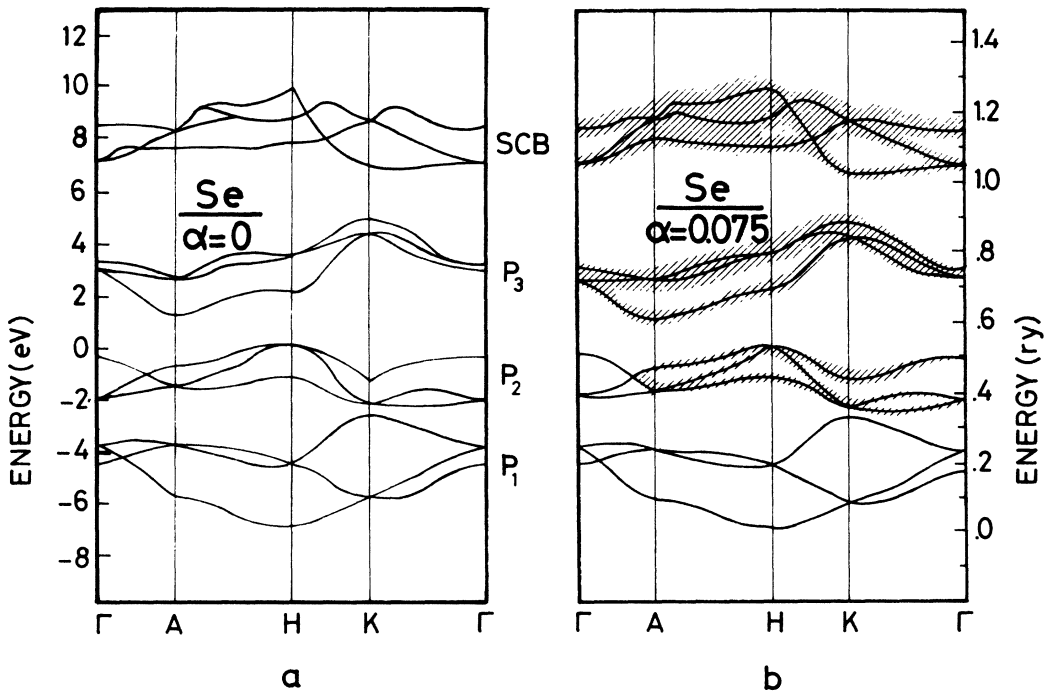

FIG. 6. Band structure of Se. (a) $\alpha = 0$ crystalline case (see also Ref. 15); (b) $\alpha = 0.075$ (see also Ref. 4). Explanation of the figure is the same as for Te.

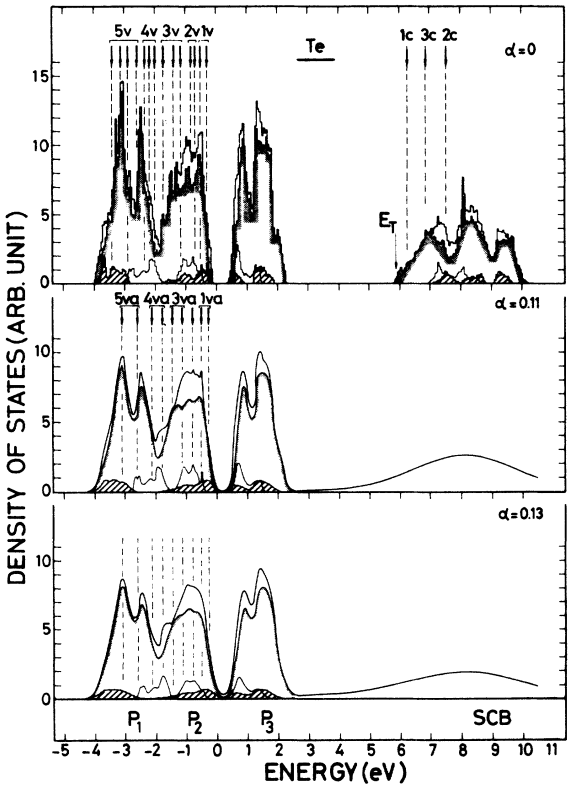

FIG. 7. Density of states of Te for different stages of disorder, i.e., different values of α. The density of states contributed by the total Brillouin zone is shown as a heavy line (heavy histogram in the DOS for $\alpha = 0$). The DOS contributed by the region near the Δ axis (see text) is shown as a thin line. The dashed partial contribution is the DOS contributed by the region near point H (see text). The DOS contributed by the rest of the BZ (= total BZ region near Δ region near H) is shown as a shadowed line. The average imaginary parts of energy used in the calculations for $\alpha \neq 0$ are listed in Table III. The arrows denote the positions of structures in DOS (total DOS or one of the contributions) as resulting from the experiment (see Paper II). The photoelectric threshold E_T is assumed to be at the bottom of the second conduction band (5.8 eV).

exhibits the same over-all behavior upon disorder as that of Te. Again, the Δ contribution gives rise to fine structures in the p bands up to $\alpha = 0.10$. The only essential difference with Te is that there remains still a small bump in the second conduction band up to $\alpha = 0.10$, owing to small imaginary parts of energy near the band edge as compared to the rest of the band [see also Fig. 6 and Table II(b)].

V. CONCLUSIONS

The electronic band structures and densities of states of crystalline and amorphous Te and Se have been calculated. In the crystalline cases, the results are valid within the limitations of the energy-independent local atomic-model potential and the convergency uncertainties. The crystalline energy spectra are already tested by calculating the respective ϵ_2 spectra and comparing them with optical-absorption results.[15,16] It will be shown in the following paper, that we can also interpret the crystalline photoemission data by using these results.

For the amorphous cases the situation is somewhat different. Besides the model-potential approximation, we made three additional assumptions:

(i) We took the n-atom correlation function D_n to be a product of two-atom correlation functions [Eq. (9)]. This implies a neglect of multiple scattering associated with more than one atom. However, these multiple scatterings are taken into account approximately by assuming the two-atom correlation function to be angular dependent and to consist of a sum of relatively sharp peaks.[48] These assumptions are not strictly justified, but might be taken to be reasonable when restricting our considerations to the density of states well within the bands.

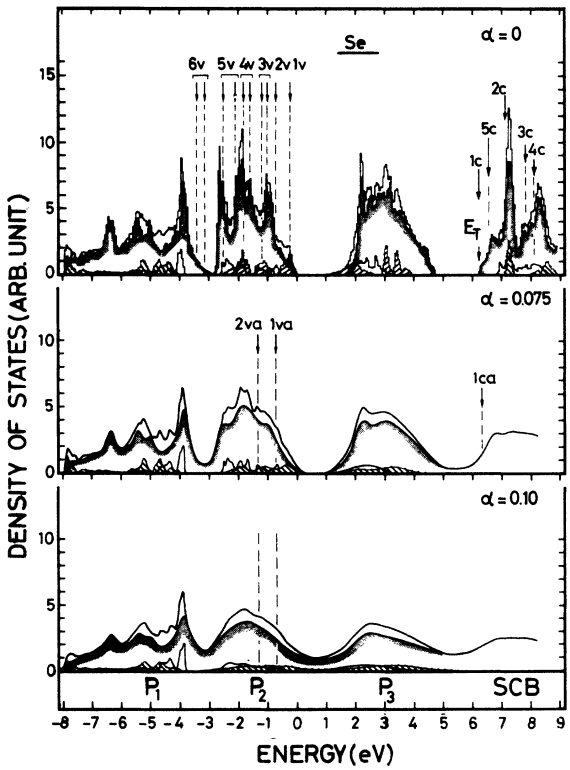

FIG. 8. The density of states of Se for different stages of disorder. The explanation of the figure is the same as for Te. Again, the photoelectric threshold is assumed to be at the bottom of the second conduction band (6.2 eV).

(ii) The Fourier-transformed atomic potential $v(\vec{q})$ was taken to be constant near $\vec{q} - \vec{K}_{n'}$ when performing the $\vec{k}$ integrations in the infinite series of the averaged Green's function.[41] This may be justified for small values of the disorder parameter α and should not effect our results up to $\alpha = 0.10$.

(iii) The short-range order present in the amorphous phases was taken to be the same as in the trigonal phases. This is justified when considering the experimental two-atom distribution function of Se, where the mean distance between next-nearest neighbors in the amorphous phase is seen to be the same as in the crystal. However, for the second-, third-, etc , nearest neighbors there are deviations from the trigonal distance. These deviations can be explained by assuming the amorphous Se phase to consist partly of Se_8 rings.[30,31] Therefore, we may only expect the gross features of the amorphous DOS to be reproduced satisfactorily by our approach. In the case of Te, only one quantitative structural measurement on the amorphous phase is available. From this, one may conclude that only the nearest neighbors are described correctly by our model. The comparison of the calculated DOS with the results of the photoemission experiments described in the following paper[25] will allow us to test whether our structural model is reasonable or not.

One of the main results of the present DOS calculations is that in both materials the over-all shape of the three p bands is almost identical in the crystalline and the amorphous phases, whereas the second conduction band DOS is smeared out almost completely. This gives rise to the conclusion that the shapes, positions, and widths of the three p bands are mainly determined by short-range order effects, i.e., the arrangement of one atom with its nearest and perhaps next-nearest neighbors. Most of the fine structure that is preserved in the valence bands when increasing disorder is related to the Δ contribution to the DOS. Therefore, one may conclude, that this partial DOS is connected with the next-nearest-neighbor configuration.

It is interesting to compare our DOS results in the case of Te with the results obtained by Hartmann and Mahanti,[55] who used a tight-binding approximation taking into account the correlation between the nearest and next-nearest neighbors within the same chain. In this approach, the positions of the nearest neighbors are taken to be fixed and to correspond exactly to the trigonal configuration, whereas the bond parameters from the nearest to the next-nearest neighbors are varied. The resulting DOS of the three p bands agrees only qualitatively with the result of our calculation. The p_2 band exhibits three relatively sharp peaks that do not appear in the p_2 band of Fig. 7, this paper, for $\alpha = 0.11$ and $\alpha = 0.13$. The p_1 and p_3 bands in[55] consist of only one broad peak with a small shoulder on the high-energy edge, whereas in Fig. 7 both bands exhibit two peaks even for relatively large values of α. It is probable, that the three sharp peaks in the p_2 band are correlated with the fact that the next-nearest-neighbors configuration is taken to be exactly that of the trigonal crystal, in contrast with the actual structural model (Fig. 3), where disorder effects even the first-nearest neighbors. It would be interesting to have a DOS calculation for trigonal Te based on the same approach as in Ref. 55. This would allow us to study the disorder behavior of the three p bands in tight-binding approach, and to compare it to our results in Fig. 7.

Recently, a calculation of the density of states of amorphous Se was performed using a molecular-orbital approach.[56] Two different structural models were used in these calculations: The density of states obtained with the trigonal (chain) model agrees qualitatively with our result for $\alpha = 0.10$ in Fig. 8 in the energy region of the p_2 and the upper part of the p_1 band. The density of states calculated by using a monoclinic (ring) model differs in peak positions and strengths. A comparison of the molecular-orbital results with photoemission data (energy distribution curves-EDC)[56,57] shows that only the chain model allows for a reasonable fit to the experimental results. Therefore we expect that we will be able to also interpret the high-resolution photoemission data of the following paper by using our trigonal structural model.

ACKNOWLEDGMENTS

The authors gratefully acknowledge helpful discussions with Professor J. Treusch. Two of us (K. M. and B. K.) are indebted to the Deutsche Forschungsgemeinschaft for financial support during the course of this work.

[1] P. Grosse, Springer Tracts Mod. Phys. 48, 66 (1969).
[2] J. Stuke, in *Proceedings of the International Symposium on Se and Te, Montreal, 1967,* edited by C. Cooper (Pergamon Oxford, England, 1969), p. 3; see also Chaps. II and IV.
[3] G. Lucovsky, R. C. Keezer, and E. Burstein, Solid State Commun. **5**, 439 (1967).
[4] S. Tutihasi, G. G. Roberts, R. C. Keezer, and R. E. Drews, Phys. Rev. **177**, 1143 (1969).
[5] R. Geick, M. Schröder, and J. Stuke, Phys. Status Solidi **24**, 99 (1967).
[6] G. G. Roberts, S. Tutihasi, and R. C. Keezer, Phys. Rev. **166**, 637 (1968).
[7] R. Fischer, Phys. Status Solidi **31**, K139 (1969).
[8] J. Stuke and H. Keller, Phys. Status Solidi **7**, 189 (1964).

[9]E. Mohler, J. Stuke, and G. Zimmerer, Phys. Status Solidi **22**, K49 (1967).
[10]W. Henrion, Phys. Status Solidi **20**, K145 (1967).
[11]S. Tutihasi and I. Chen, Phys. Rev. **158**, 623 (1967).
[12]G. Weiser and J. Stuke, in *Proceedings of the International Conference on the Physics of Semiconductors*, edited by S. M. Ryvkin (Nauka, Moscow, 1968), p. 38.
[13]A. G. Leiga, J. Opt. Soc. Am. **58**, 880 (1968).
[14]J. Treusch and R. Sandrock, Phys. Status Solidi **16**, 487 (1966).
[15]R. Sandrock, Phys. Rev. **169**, 642 (1968).
[16]K. Maschke, Phys. Status Solidi **47**, 511 (1971).
[17]M. Hulin, Ann. Phys. (Paris) **8**, 647 (1963).
[18]M. Hulin, J. Phys. Chem. Solids **27**, 441 (1966).
[19]M. Picard and M. Hulin, Phys. Status Solidi **23**, 363 (1967).
[20]O. Betbeder-Matibet and M. Hulin, Phys. Status Solidi **36**, 573 (1969).
[21]T. Doi, K. Nakao, and H. Kamimura, J. Phys. Soc. Jap. **28**, 36 (1970); J. Phys. Soc. Jap. **28**, 822 (1970); J. Phys. Soc. Jap. **30**, 1400 (1971).
[22]B. Sonntag, T. Tuomi, and G. Zimmerer, Phys. Status Solidi B **58**, 101 (1973).
[23]E. O. Kane, Phys. Rev. **175**, 1039 (1968).
[24]U. Gerhard, Adv. Sol. State Phys. **10**, 175 (1970).
[25]L. D. Laude, B. Kramer, and K. Maschke, following paper, Phys. Rev. B 8, 5794 (1973).
[26]J. Treusch, Adv. Sol. State Phys. **7**, 18 (1967).
[27]U. Rössler and J. Treusch, Rep. Prog. Phys. **35**, 883 (1972).
[28]R. Sandrock, Adv. Sol. State Phys. **10**, 283 (1970).
[29]H. Krebs, Adv. Sol. State Phys. **9**, 1 (1969).
[30]R. Kaplov, T. A. Rowe, and B. L. Averbach, Phys. Rev. **168**, 1068 (1968).
[31]H. Richter and G. Breitling, Z. Naturforsch. A **26**, 1699 (1971).
[32]G. Lucovsky, Mater. Res. Bull. **4**, 505 (1969).
[33]G. Lucovsky, in Ref. 2, p. 255.
[34]A. Axmann, W. Gissler, and T. Springer, in Ref. 2, p. 299.
[35]M. H. Brodsky, R. J. Gambino, J. E. Smith, Jr., and Y. Yakoby, Phys. Status Solidi B **52**, 609 (1972).
[36]H. E. Swanson and E. Tatge, NBS Report No. 2202, 1951 (U.S. GPO, Washington, D.C., 1951).
[37]H. E. Swanson, W. T. Gilfrich, and G. M. Ugrinic, NBS Circular No. 539 (U.S. GPO, Washington, D.C., 1955), Vol. V.
[38]P. Cherin and P. Unger, Acta Crystallogr. **23**, 670 (1967).
[39]T. Ichikawa, J. Phys. Soc. Jap. **33**, 1729 (1972); Phys. Status Solidi **56**, 707 (1973).
[40]B. Kramer, K. Maschke, P. Thomas, and J. Treusch, Phys. Rev. Lett. **25**, 1020 (1970).
[41]B. Kramer, Phys. Status Solidi **41**, 649 (1970).
[42]B. Kramer, Phys. Status Solidi **41**, 725 (1970).
[43]B. Kramer, Phys. Status Solidi **47**, 501 (1971); see also B. Kramer, K. Maschke, and P. Thomas, Phys. Status Solidi **48**, 635 (1971); Phys. Status Solidi **49**, 525 (1972); J. Non-Cryst. Solids **8–10**, 659 (1972).
[44]K. M. Watson, Phys. Rev. **105**, 1388 (1957).
[45]F. Yonezawa and T. Matsubara, Prog. Theor. Phys. **35**, 357 (1966).
[46]F. Yonezawa and T. Matsubara, Prog. Theor. Phys. **35**, 759 (1966).
[47]P. Lloyd, Proc. Phys. Soc. Lond. **90**, 217 (1967).
[48]K. Maschke and P. Thomas, Phys. Status Solidi **39**, 453 (1970).
[49]P. O. Löwdin, J. Chem. Phys. **19**, 1396 (1951).
[50]K. Maschke and P. Thomas, Phys. Status Solidi **41**, 743 (1970).
[51]L. D. Laude, B. Fitton, B. Kramer, and K. Maschke, Phys. Rev. Lett. **27**, 1053 (1971).
[52]M. H. Cohen and T. K. Bergstresser, Phys. Rev. **141**, 789 (1966).
[53]A. O. E. Animalu and V. Heine, Philos. Mag. **12**, 1249 (1965); A. O. E. Animalu, Cavendish Laboratory Report (unpublished).
[54]J. Stuke, Adv. Sol. State Phys. **9**, 46 (1969).
[55]W. H. Hartmann and S. D. Mahanti, J. Non-Cryst. Solids **8–10**, 633 (1972).
[56]I. Chen, Phys. Rev. B **7**, 3672 (1973).
[57]P. Nielsen, Phys. Rev. **6**, 3739 (1972).

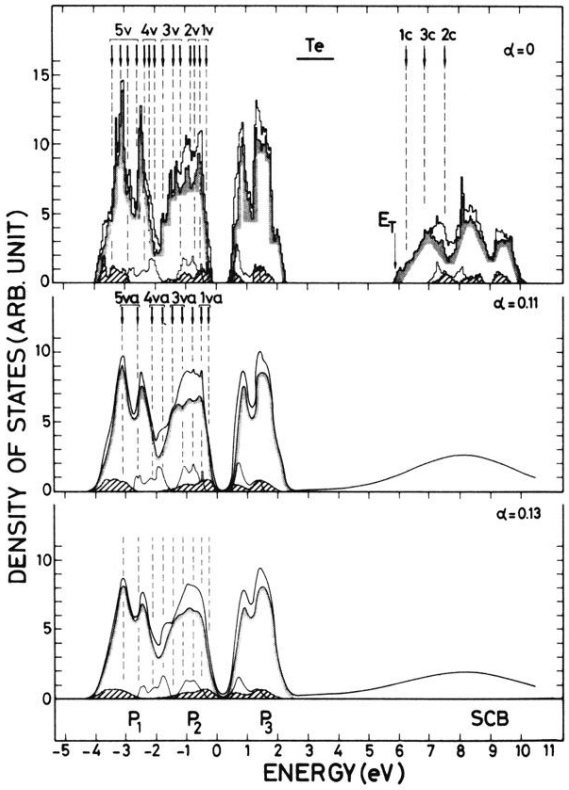

FIG. 7. Density of states of Te for different stages of disorder, i.e., different values of α. The density of states contributed by the total Brillouin zone is shown as a heavy line (heavy histogram in the DOS for $\alpha = 0$). The DOS contributed by the region near the Δ axis (see text) is shown as a thin line. The dashed partial contribution is the DOS contributed by the region near point H (see text). The DOS contributed by the rest of the BZ (= total BZ region near Δ region near H) is shown as a shadowed line. The average imaginary parts of energy used in the calculations for $\alpha \neq 0$ are listed in Table III. The arrows denote the positions of structures in DOS (total DOS or one of the contributions) as resulting from the experiment (see Paper II). The photoelectric threshold E_T is assumed to be at the bottom of the second conduction band (5.8 eV).

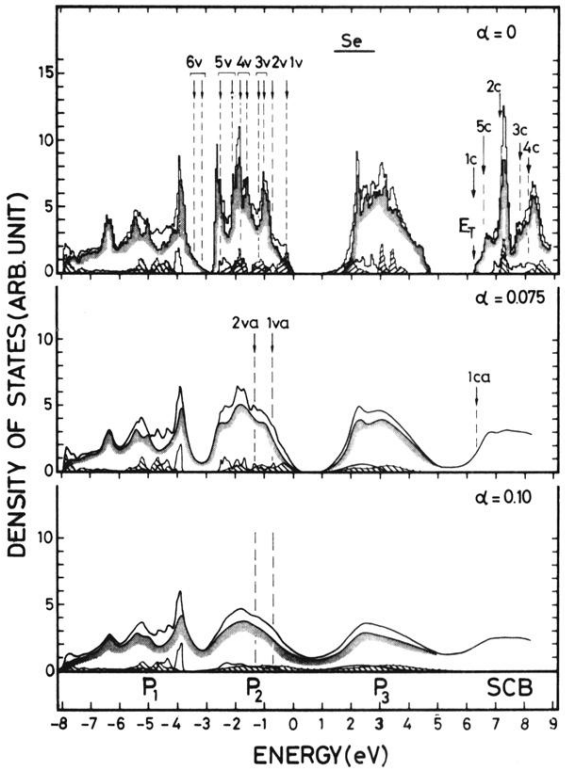

FIG. 8. The density of states of Se for different stages of disorder. The explanation of the figure is the same as for Te. Again, the photoelectric threshold is assumed to be at the bottom of the second conduction band (6.2 eV).